Computational Studies of Nonbonded Sulfur–Oxygen and Selenium–Oxygen Interactions in the Thiazole and Selenazole Nucleosides

F. Temple Burling and Barry M. Goldstein*

Contribution from the Department of Biophysics, University of Rochester Medical Center, Rochester, New York 14642. Received July 10, 1991

Abstract: Computational studies have been performed to investigate the origin and magnitude of a biologically important nonbonded interaction: the sulfur–oxygen and selenium–oxygen interaction observed in the thiazole and selenazole nucleosides. Crystallographic studies of the antitumor agents tiazofurin and selenazofurin and their analogues have demonstrated close contacts between the thiazole sulfur or selenazole selenium and the furanose oxygen. Crystallographic evidence that these contacts result from a true intramolecular interaction is reviewed. Computational findings indicate that these contacts are the result of an attractive electrostatic interaction between a positively charged heteroatom and a negatively charged oxygen. This hypothesis is supported by examination of geometry optimizations, population analyses, and molecular electrostatic isopotential maps obtained from ab initio computations (RHF/STO-3G, 3-21G, 3-21G*, and 6-31G* levels) for both isolated thiazole and selenazole rings and for model nucleoside fragments. Semiempirical (MNDO) computations on the thiazole nucleosides estimate that this attractive sulfur–oxygen interaction, in combination with a repulsive nitrogen–oxygen interaction, produces a barrier to rotation about the C–glycosidic bond of ~4 kcal/mol.

I. Introduction

"Nonbonded" interactions play a significant role in structural chemistry. Attractive, albeit noncovalent interactions modulate the conformations of virtually all molecular assemblies. The influence of electrostatic and dispersive forces on conformation in biological macromolecules offers a well-known example.[1] Nonbonded intermolecular interactions between small molecules in the solid state have also been investigated.[2-4] In this study, we examine the origins of an attractive 1,4 intramolecular interaction of divalent sulfur and selenium with oxygen. This interaction is consistently observed in an unusual class of biologically active molecules: the thiazole and selenazole nucleosides.

The thiazole nucleoside tiazofurin (2-β-D-ribofuranosyl-thiazole-4-carboxamide, NSC286193, Figure 1a) is a widely studied agent with a diverse array of biological effects. These include clinically effective antitumor activity,[5,6] the ability to induce differentiation in neoplastic cells,[7-10] and the ability to inhibit G protein-mediated cellular signaling mechanisms[10-12] and down-regulate oncogene activity.[13] Crystal structures of tiazofurin and eight inactive thiazole nucleoside analogues all exhibit 1,4 close contacts between the thiazole sulfur and furanose oxygen O1'.[14-17]

Observed S–O1' distances lie in the range 2.77–3.16 Å (see below), and in all cases are less than the sum of the sulfur and oxygen van der Waals radii (3.3 Å).[18] Selenazofurin (2-β-D-ribo-furanosylselenazole-4-carboxamide, NSC 340847, Figure 1b) is the selenium analogue of tiazofurin. Selenazofurin shows both antitumor[19-21] and antiviral activity,[22,23] as well as efficacy as a maturation-inducing agent.[7,11,12,24] The crystal structures of selenazofurin and its α anomer show selenium–oxygen contacts of 3.012 Å and 2.888 Å, respectively.[25] These contacts are also less than the sum of the selenium and oxygen van der Waals radii (3.40 Å).[18]

Close contacts between the thiazole or selenazole heteroatom and the furanose oxygen have been attributed to an attractive S/Se–O interaction. Biological implications of this interaction have been proposed.[25,26] The various biological effects of tiazo- and selenazofurin appear related to a shutdown of guanine nucleotide synthesis[5-9,24] produced by dinucleotide anabolites of the parent compounds.[27-29] In vivo, tiazo- and selenazofurin are

(1) See, for example: Cantor, C. R.; Schimmel, P. R. *Biophysical Chemistry Part I: The Conformation of Biological Macromolecules*; W. H. Freeman: New York, 1980; Chapter 5.

(2) Ramasubbu, N.; Parthasarathy, R. *Phosphorus Sulfur* **1987**, *31*, 221-229.

(3) Guru Row, T. N.; Parthasarathy, R. *J. Am. Chem. Soc.* **1981**, *103*, 477-479.

(4) Rosenfield, R. E.; Parthasarathy, R.; Dunitz, J. D. *J. Am. Chem. Soc.* **1977**, *99*, 4860-4862.

(5) Tricot, G. J.; Jayaram, H. N.; Lapis, E.; Natsumeda, Y.; Nichols, C. R.; Kneebone, P.; Heerema, N.; Weber, G.; Hoffman, R. *Cancer Res.* **1989**, *49*, 3696-3701.

(6) Tricot, G. J.; Jayaram, H. N.; Nichols, C. R.; Pennington, K.; Lapis, E.; Weber, G.; Hoffman, R. *Cancer Res.* **1987**, *47*, 4988-4991.

(7) Goldstein, B. M.; Leary, J. F.; Farley, B. A.; Marquez, V. E.; Levy, P. C.; Rowley, P. T. *Blood* **1991**, *78*, 593-598.

(8) Kiguchi, K.; Collart, F. R.; Henning-Chubb, C.; Huberman, E. *Exp. Cell Res.* **1990**, *187*, 47-53.

(9) Collart, F. R.; Huberman, E. *Blood* **1990**, *75*, 570-576.

(10) Olah, E.; Natsumeda, Y.; Ikegami, T.; Kote, Z.; Horany, M.; Szelenyi, J.; Paulik, E.; Kremmer, T.; Hollan, S. R.; Sugar, J.; Weber, G. *Proc. Natl. Acad. Sci.* **1988**, *85*, 6533-6537.

(11) Parandoosh, Z.; Rubalcava, B.; Matsumoto, S. S.; Jolley, W. B.; Robins, R. K. *Life Sci.* **1990**, *46*, 315-320.

(12) Parandoosh, Z.; Robins, R. K.; Belei, M.; Rubalcava, B. *Biochem. Biophys. Res. Commun.* **1989**, *164*, 869-874.

(13) Kharbanda, S. M.; Sherman, M. L.; Kufe, D. W. *Blood* **1990**, *75*, 583-588.

(14) Goldstein, B. M.; Takusagawa, F.; Berman, H. M.; Srivastava, P. C.; Robins, R. K. *J. Am. Chem. Soc.* **1983**, *105*, 7416-7422.

(15) Goldstein, B. M.; Mao, D. T.; Marquez, V. E. *J. Med. Chem.* **1988**, *31*, 1026-1031.

(16) Burling, F. T.; Gabrielsen, B.; Goldstein, B. M. *Acta Crystallogr., Sect. C* **1991**, *C47*, 1272-1275.

(17) Burling, F. T.; Hallows, W. H.; Phelan, M. J.; Gabrielsen, B.; Goldstein, B. M. *Acta Crystallogr.*, in press.

(18) Bondi, A. *J. Phys. Chem.* **1964**, *68*, 441-451.

(19) Boritzki, T. J.; Berry, D. A.; Besserer, J. A.; Cook, P. D.; Fry, D. W.; Leopold, W. R.; Jackson, R. C. *Biochem. Pharmacol.* **1985**, *34*, 1109-1114.

(20) Berger, N. A.; Berger, S. J.; Catino, D. M.; Petzold, S. J.; Robins, R. K. *J. Clin. Invest.* **1985**, *75*, 702-709.

(21) Srivastava, P. C.; Robins, R. K. *J. Med. Chem.* **1983**, *26*, 445-448.

(22) Sidwell, R. W.; Huffman, J. H.; Call, E. W.; Alaghamandan, H.; Cook, P. D.; Robins, R. K. *Antimicrob. Agents Chemother.* **1985**, *28*, 375-377.

(23) Kirsi, J. J.; North, J. A.; McKernan, P. A.; Murray, B. K.; Canonico, P. G.; Huggins, J. W.; Srivastava, P. C.; Robins, R. K. *Antimicrob. Agents Chemother.* **1983**, *24*, 353-361.

(24) Sokoloski, J. A.; Blair, O. C.; Sartorelli, A. C. *Cancer Res.* **1986**, *46*, 2314-2319.

(25) Goldstein, B. M.; Takusagawa, F.; Berman, H. M.; Srivastava, P. C.; Robins, R. K. *J. Am. Chem. Soc.* **1985**, *107*, 1394-1400.

(26) Goldstein, B. M.; Bell, J. E.; Marquez, V. E. *J. Med. Chem.* **1990**, *33*, 1123-1127.

(27) Jayaram, H. N.; Ahluwalia, G. S.; Dion, R. L.; Gebeyehu, G.; Marquez, V. E.; Kelley, J. A.; Robins, R. K.; Cooney, D. A.; Johns, D. G. *Biochem. Pharmacol.* **1983**, *32*, 2633-2636.

(28) Cooney, D. A.; Jayaram, H. N.; Gebeyehu, G.; Betts, C. R.; Kelly, J. A.; Marquez, V. E.; Johns, D. G. *Biochem. Pharmacol.* **1982**, *31*, 2133-2136.

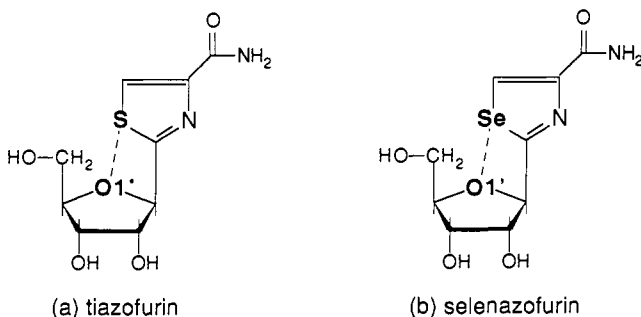2314 *J. Am. Chem. Soc., Vol. 114, No. 7, 1992*

Burling and Goldstein

Figure 1. The thiazole nucleoside tiazofurin (a) and its selenium analogue selenazofurin (b). Dotted lines represent the observed close contacts between the base heteroatom (S or Se) and the furanose oxygen (O1′).

Figure 2. Intramolecular S–O1′ distances versus S–C2–C1′ bond angles (∠C2) for the crystal structures of the tiazofurin analogues listed in Table I.

anabolized to the dinucleotides TAD and SAD, respectively (thiazole- and selenazole-4-carboxamide adenine dinucleotides). These dinucleotides act as inhibitors of inosine monophosphate dehydrogenase (IMPd), the enzyme catalyzing the rate-limiting step in guanine nucleotide synthesis.[30] A significant heteroatom–oxygen interaction would constrain rotation about the C-glycosidic bond in TAD and SAD. This in turn would influence specificity of binding of these active tiazo- and selenazofurin anabolites to the target enzyme.[25,26]

In the solid state, a close intramolecular contact may result from either an attractive intramolecular interaction or from external forces imposed by crystal packing. Observation of the same contacts in different packing environments supports the presence of an intramolecular interaction. Examples of close intramolecular contacts between nonbonded atoms are found throughout the crystallographic literature, but systematic studies among related series of compounds are rare. A 1985 survey of the Cambridge Crystallographic Database revealed 750 structures containing close intramolecular sulfur–oxygen contacts between 2.00 and 3.25 Å.[31] Of these, 150 structures contained divalent sulfur (S(II)) and oxygen atoms in 1,4 positions. A more recent survey of this data base[32] yielded 144 additional structures containing intramolecular S–O 1,4 contacts less than 3.3 Å. Analogous intramolecular selenium–oxygen contacts less than 3.4 Å are seen in only 14 structures.[32]

Qualitative interpretations of S/Se–O interactions have been based on both electrostatic[14,33] and frontier orbital[34,35] arguments. However, relatively little modern computational work has been done on sulfur–oxygen interactions,[34–38] and none has appeared on the selenium–oxygen system. The thiazole and selenazole nucleosides are well-defined structures of biological interest in which the close heteroatom–oxygen interaction is of potential importance. We have thus performed a series of quantum-mechanical-based computations in an effort to identify the origin of the heteroatom–oxygen interaction in this class of compounds.

First, crystallographic evidence for this interaction is reviewed. Next, ab initio computations are used to examine the detailed electronic structure of both isolated thiazole and selenazole heterocycles, and model nucleoside fragments. Hypotheses developed from these studies are then examined using semiempirical methods applied to larger fragments. Results suggest that close heteroatom–oxygen contacts arise from an attractive electrostatic interaction between a positively charged sulfur or selenium and a negatively charged O1′ oxygen.

II. Methods

All calculations were performed using the University of Rochester's Alliant FX-80 and the Cornell National Supercomputing Facility's IBM 3090.

Ab initio calculations were performed using the GAUSSIAN86[39] and GAUSSIAN88[40] program systems and associated basis sets. Ab initio calculations were performed at the RHF level of theory using either STO-3G, 3-21G, 3-21G*, and/or 6-31G* basis sets[41] for the sulfur-containing systems and STO-3G for the selenium-containing systems. The particular level of theory for each computation is indicated in the text and appropriate figure caption. Geometry optimizations used the analytical gradient method.[39,40] Population analyses were carried out using the Pop = Full option.[39,40] Electrostatic isopotential maps were computed using the Prop = Grid option.[39,40] Values of the potential were computed over a 15 × 15 × 15 array of points surrounding the fragment of interest. The spacing between these points was 0.5 Å for the isolated heterocycles and 0.6 Å for the larger fragments. Maps were displayed on an Evans and Sutherland PS330 using the CHEMX suite of programs[42] and local interface software.

Semiempirical calculations were performed using both the AMPAC[43] and MOPAC[44] program systems. Only sulfur-containing fragments were examined, due to parameter set limitations. Calculations were done using both MNDO[45] and PM3[46] parameter sets. Results were qualitatively similar, although MNDO-derived results were in general more consistent with those obtained via ab initio methods for these systems. Thus the MNDO results are presented. Geometry optimization was performed

(29) Kuttan, R.; Robins, R. K.; Saunders, P. P. *Biochem. Biophys. Res. Commun.* 1982, *107*, 862–868.

(30) Jackson, R. C.; Weber, G.; Morris, H. P. *Nature* 1975, *256*, 331–333.

(31) Kucsman, A.; Kapovits, I. Nonbonded Sulfur-oxygen Interaction in Organic Sulfur Compounds. In *Organic Sulfur Chemistry*; Bernardi, F., Csizmadia, I. G., Mangini, A., Eds.; Elsevier: Amsterdam, 1985; pp 191–245 and references therein.

(32) Burling, F. T.; Goldstein, B. M., in preparation.

(33) Goldstein, B. M.; Kennedy, S. D.; Hennen, W. J. *J. Am. Chem. Soc.* 1990, *112*, 8265–8268.

(34) Becker, P.; Cohen-Addad, C.; Delley, B.; Hirshfeld, F. L.; Lehmann, M. S. A Theoretical Study of Short S–O "Non-bonded" Interactions. In *Applied Quantum Chemistry*; Smith, V. H., Jr., Schaefer, H. F., III, Morokuma, K., Eds.; D. Reidel: Boston, 1986; pp 361–373.

(35) Cohen-Addad, C.; Lehmann, M. S.; Becker, P.; Párkányi, L.; Kálmán, A. *J. Chem. Soc., Perkin Trans. 2* 1984, 191–196.

(36) Barbieri, G.; Benassi, R.; Taddei, F. *J. Mol. Struct.* 1989, *184*, 269–276.

(37) de Barbeyrac, J. P.; Gonbeau, D.; Pfister-Guillouzo, G. *J. Mol. Struct.* 1973, *16*, 103–115.

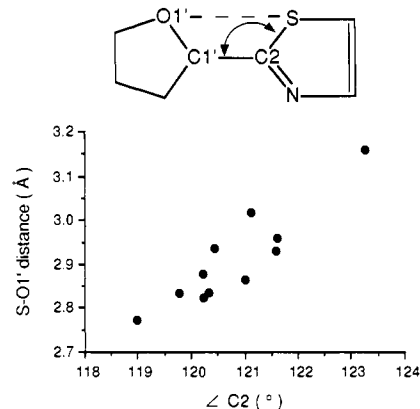(38) Kapecki, J. A.; Baldwin, J. E. *J. Am. Chem. Soc.* 1969, *91*, 1120–1123.

(39) GAUSSIAN86: Frisch, M. J.; Binkley, J. S.; Schlegel, H. B.; Raghavachari, K.; Melius, C. F.; Martin, R. L.; Stewart, J. J. P.; Bobrowicz, F. W.; Rohlfing, C. M.; Kahn, L. R.; Defrees, D. J.; Seeger, R.; Whiteside, R. A.; Fox, D. J.; Fleuder, E. M.; Pople, J. A. Carnegie-Mellon Quantum Chemistry Publishing Unit: Pittsburgh, PA, 1984.

(40) GAUSSIAN88: Frisch, M. J.; Head-Gordon, M.; Schlegel, H. B.; Raghavachari, K.; Binkley, J. S.; Gonzalez, C.; Defrees, D. J.; Fox, D. J.; Whiteside, R. A.; Seeger, R.; Melius, C. F.; Baker, J.; Martin, R. L.; Kahn, L. R.; Stewart, J. J. P.; Fleuder, E. M.; Topiol, S.; Pople, J. A. Gaussian, Inc.: Pittsburgh, PA, 1988.

(41) Hehre, W. J.; Radom, L.; Schleyer, P. v. R.; Pople, J. A. *Ab Initio Molecular Orbital Theory*; Wiley: New York, 1986; Chapter 4.

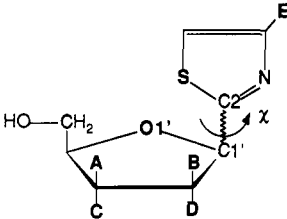(42) CHEMX, developed and distributed by Chemical Design Ltd., Oxford, England.

(43) Dewar Research Group: Stewart, J. J. P. AMPAC (QCPE 506) *QCPE Bull.* 1986, *6*, 24.

(44) Stewart, J. J. P. MOPAC (QCPE 455) *QCPE Bull.* 1989, *9*, 10–15.

(45) (a) Dewar, M. J. S.; Thiel, W. *J. Am. Chem. Soc.* 1977, *99*, 4899–4907. (b) Dewar, M. J. S.; Reynolds, C. H. *J. Comput. Chem.* 1986, *7*, 140–143.

(46) Stewart, J. J. P. *J. Comput. Chem.* 1989, *10*, 209–220.

Table I. S–O1′ Contacts Observed in Thiazole Nucleoside Structures

compound	S–O1′ dis (Å)	torsion angle χ (deg)	C-glycosidic linkage	A	B	C	D	E	ref
4-methylamidate TF (mol A)	2.773 (2)	15.6 (3)	β	H	H	OH	OH	–C(OCH₃)NH	17
α-TF	2.826 (3)	–20.8 (3)	α	H	H	OH	OH	–CONH₂	14
2′,3′-dideoxy TF	2.834 (2)	14.1 (2)	β	H	H	H	H	–CONH₂	16
2′,3′-dideoxy-2′,3′-didehydro TF	2.835 (1)	5.2 (3)	β	H	H			–CONH₂	16
xylo-TF (mol A)	2.865 (2)	21.8 (4)	β	OH	H	H	OH	–CONH₂	32
4-methylamidate TF (mol B)	2.878 (2)	27.2 (3)	β	H	H	OH	OH	–C(OCH₃)NH	17
xylo-TF (mol B)	2.929 (3)	30.1 (3)	β	OH	H	H	OH	–CONH₂	32
4-cyano TF	2.936 (3)	34.5 (4)	β	H	H	OH	OH	–CN	17
tiazofurin (TF)	2.958 (1)	30.7 (1)	β	H	H	OH	OH	–CONH₂	14
2′-deoxy TF	3.018 (3)	40.8 (2)	β	H	H	OH	H	–CONH₂	14
ara-TF	3.158 (4)	55.2 (5)	β	H	OH	OH	H	–CONH₂	15

using the default method and all computations employed the PRECISE keyword.⁴³,⁴⁴

Profiles of total electronic energy of a given fragment as a function of C–glycosidic torsion angle χ were obtained as follows. The value of χ was incremented in 20° steps and fixed. The remainder of all geometry variables describing the fragment were then optimized. All curves associated with fragments of different chemical compositions plotted on the same axes were normalized to the same global minimum. For all computations, a value of χ = 0° refers to the conformation in which the sulfur (selenium) and oxygen atoms are cis planar. A positive value of χ indicates a counterclockwise rotation of the C2–S(Se) bond relative to the C1′–O1′ bond when viewed down the glycosidic bond from C2 to C1′. Additional details associated with specific computations are given in the body of the text and figure captions.

III. Crystallographic Studies

Evidence for the existence of a sulfur–oxygen interaction is seen in 11 crystal structures of 9 different thiazole nucleosides (two of these compounds crystallized with two independent molecules per asymmetric unit). These data are summarized in Table I, which lists the S–O1′ distance and the associated glycosidic torsion angle χ = S–C2–C1′–O1′ for each of the thiazole nucleoside crystal structures determined to date. The torsion angle χ describes the conformation of the thiazole ring about the glycosidic bond and lies within the range 5.2–55.2°. In each structure the thiazole sulfur lies cis to the pentose O1′ oxygen. S–O1′ distances are 2.773–3.158 Å, all less than the 3.3 Å sum of S and O van der Waals radii.¹⁸ The largest glycosidic angle, χ = 55.2°, is observed in ara-tiazofurin, which exhibits only a moderately close S–O1′ contact (3.158 Å). This observation will be addressed below. Nevertheless, the presence of close S–O contacts in 11 crystallographically independent molecules suggests that these are due to a true intramolecular interaction and are not artifacts of crystal packing.

Additional evidence for a nonbonded sulfur–oxygen interaction in the thiazole nucleosides is shown in Figure 2. Here we plot the S–O1′ distance and corresponding S–C2–C1′ bond angle for each structure listed in Table I. Figure 2 indicates that the bond angle about carbon C2 on the thiazole ring decreases as the S–O1′ distance shortens. In the absence of an attractive S–O interaction, the S–C2–C1′ angle would be expected to increase with decreasing S–O distances. This would relieve the steric strain produced by the closer S–O contacts. The closing of this bond angle is a further indication of the presence of an interaction which serves to "pull" the thiazole sulfur toward the O1′ oxygen.

IV. Ab Initio Computational Studies

A. Thiazole and Selenazole Heterocycles. Before investigating the sulfur–oxygen and selenium–oxygen interaction per se, computations were carried out on isolated thiazole and selenazole rings
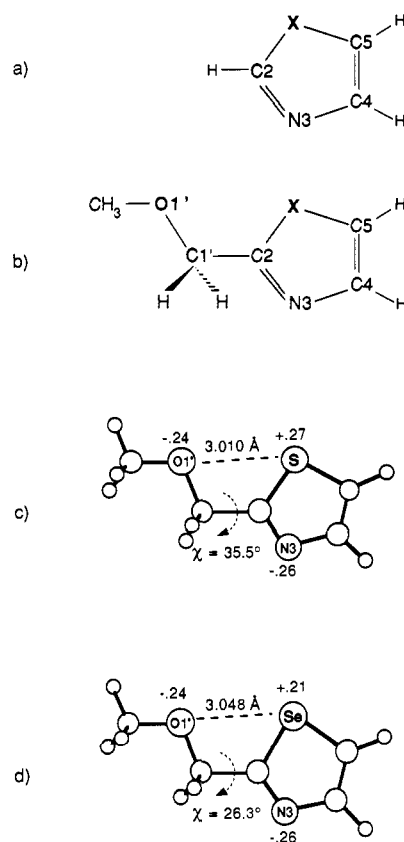
Figure 3. (a) Isolated thiazole (X = S) and selenazole (X = Se) heterocycle used in the computations summarized in Table II. (b) Thiazole (X = S) and selenazole (X = Se) nucleoside core fragment. (c) STO-3G minimized geometry of the thiazole nucleoside core fragment. Mulliken charges shown for O1′, S, and N3 are from the STO-3G computation (RHF/STO-3G//STO-3G level). A 3-21G* single-point calculation (RHF/3-21G*//STO-3G level) gave Mulliken charges of –0.63, +0.46, and –0.60 for O1′, S, and N3, respectively. (d) STO-3G minimized geometry for the selenazole core fragment. Mulliken charges listed are from the STO-3G computation (RHF/STO-3G//STO-3G level).

(Figure 3a). The purpose was to examine in detail the electron distribution in these heterocycles, and the resultant electrostatic environments. Information about the electronic structure of these rings is clearly of interest in itself. Further, examination of the electron distribution in the thiazole and selenazole moieties provided a starting point from which to determine the interactions

Table II. Population Analyses for Thiazole and Selenazole Heterocycles[a]
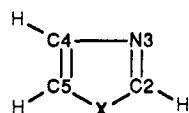
	thiazole ring (X = S)				selenazole ring (X = Se)	
	STO-3G// STO-3G	3-21G// 3-21G	3-21G*// 3-21G*	6-31G*// 6-31G*		STO-3G// STO-3G
(a) Outer Pz Orbital Overlap Populations						
S(3Pz)–C2(2Pz)	0.0401	0.0485	0.0585	0.0668	Se(4Pz)–C2(2Pz)	0.0329
S(3Pz)–C5(2Pz)	0.0353	0.0334	0.0408	0.0300	Se(4Pz)–C5(2Pz)	0.0287
C2(2Pz)–N3(2Pz)	0.1542	0.2074	0.1954	0.1958	C2(2Pz)–N3(2Pz)	0.1597
N3(2Pz)–C4(2Pz)	0.0464	0.0584	0.0739	0.0671	N3(2Pz)–C4(2Pz)	0.0415
C4(2Pz)–C5(2Pz)	0.1698	0.2301	0.2184	0.2240	C4(2Pz)–C5(2Pz)	0.1746
(b) Gross Orbital Populations						
S 3Pz	1.759	1.814	1.756	1.730	Se 4Pz	1.809
C2 2Pz	1.032	0.994	1.008	0.946	C2 2Pz	1.014
N3 2Pz	1.091	1.111	1.115	1.157	N3 2Pz	1.081
C4 2Pz	1.056	1.025	1.024	0.980	C4 2Pz	1.046
C5 2Pz	1.067	1.088	1.103	1.108	C5 2Pz	1.052
(c) Net Atomic Charges						
S	0.262	0.509	0.392	0.273	Se	0.206
C2	−0.069	−0.220	−0.136	−0.125	C2	−0.054
N3	−0.246	−0.555	−0.577	−0.438	N3	−0.238
C4	−0.008	0.074	0.038	0.040	C4	0.001
C5	−0.185	−0.663	−0.543	−0.445	C5	−0.175

[a] Note: Pz orbitals are normal to the plane of the heterocycle. The 6-31G* values include sulfur 4Pz and carbon nitrogen 3Pz orbitals.

responsible for the close contacts seen in tiazofurin and selenazofurin.

Results of Mulliken population analyses[47] obtained from ab initio calculations performed on isolated thiazole and selenazole heterocycles (Figure 3a) are summarized in Table II. Starting geometries for both heterocycles were derived from crystal structure data, followed by full geometry optimization using the STO-3G basis set.[41] The selenazole ring could only be examined at this level of theory. However, the thiazole ring was further subjected to full optimization at the 3-21G, 3-21G*, and 6-31G* levels[41] to confirm the robustness of the results from the STO-3G calculations. As discussed below, Mulliken population analyses from these calculations show that the sulfur and selenium atoms participate in π-bonding with adjacent carbon atoms in the thiazole and selenazole rings. As a result of charge delocalization due to π-bonding, the thiazole sulfur and selenazole selenium atoms carry a net positive charge.

Table IIa lists the orbital overlap populations[41,47] between the outermost Pz orbitals calculated for the thiazole and selenazole rings using several basis sets. For the 3-21G and 3-21G* calculations, the outer Pz orbital overlap populations were determined by adding the contributions from the overlap between both the inner and outer components of the Pz orbitals. The 6-31G* basis set contains 4P orbitals for sulfur and 3P orbitals for carbon and nitrogen, which allow for electron redistribution into 4Pz and 3Pz orbitals. The outer Pz overlap population listed here is a sum of the contributions from the 3Pz and 4Pz orbitals on the sulfur atom, and the 2Pz and 3Pz orbitals on the carbon and nitrogen atoms. The results from calculations on the thiazole ring are consistent for each basis set used. The data shows that the sulfur Pz orbitals share a significant amount of charge with those of the adjacent carbon atoms C2 and C5 (bold figures). This indicates participation of these orbitals in S–C2 and S–C5 π-bonding. The S–C2 overlap populations range from 0.0401 to 0.0668, while the S–C5 overlap populations range from 0.0300 to 0.0408. For comparison, these values are roughly 1/4 to 1/2 of the STO-3G overlap population between adjacent carbon 2Pz orbitals calculated for

a fully conjugated system such as benzene. The STO-3G sulfur–carbon overlap population computed for an unconjugated S–C bond, such as that found in CH_3–S–CH_3, is 0.001, an order of magnitude less than that seen in the thiazole ring. Similarly, the STO-3G calculation on the selenazole ring shows that the selenium atom 4Pz orbital shares charge with the flanking carbon 2Pz orbitals (Table IIa, bold figures). The N3–C4 bonds in both heterocycles also have large 2Pz overlap populations. Thus, both the thiazole and selenazole rings show a significant degree of conjugation.

Table IIb lists the gross orbital populations[41,47] for the outermost Pz orbitals in the thiazole and selenazole rings. The gross orbital population measures the total charge that the population analysis assigns to an individual atomic orbital. The gross orbital population of the sulfur 3Pz orbital (or 3Pz and 4Pz in the 6-31G* calculation) is decreased from 2.0 to between 1.730 and 1.814, depending on the basis set used. These numbers indicate that, as a result of π-bonding, the outermost sulfur Pz orbital loses roughly 1/5 to 1/4 of an electron to the rest of the ring. The STO-3G calculation on the selenazole ring (Table II) shows that the selenium 4Pz orbital experiences a similar decrease in electron population as a result of π-bonding.

The decrease seen in the outermost Pz orbital population in the thiazole and selenazole rings produces a net positive charge on both the sulfur and selenium atoms. Table IIc lists the calculated net atomic charges for both the thiazole and selenazole rings using several different basis sets. In all cases the sulfur and selenium atoms carry a substantial positive charge while a net negative charge is centered on the N3 nitrogen.

Several ab initio LCAO–MO[41] based computations have been performed on the thiazole heterocycle at lower levels of theory,[36,48–50] as well as a recent spin-coupled computation.[51] As far as the authors are aware, no comparable results have appeared

(47) (a) Mulliken, R. S. *J. Chem. Phys.* **1955**, *23*, 1833–1840. (b) Mulliken, R. S. *J. Chem. Phys.* **1955**, *23*, 1841–1846. (c) Mulliken, R. S. *J. Chem. Phys.* **1955**, *23*, 2338–2342. (d) Mulliken, R. S. *J. Chem. Phys.* **1955**, *23*, 2343–2346.

(48) Salmona, G.; Faure, R.; Vincent, E. J.; Guimon, C.; Pfister-Guillouzo, G. *J. Mol. Struct.* **1978**, *48*, 205–217.

(49) Palmer, M. H.; Findlay, R. H.; Ridyard, J. N. A.; Barrie, A.; Swift, P. *J. Mol. Struct.* **1977**, *39*, 189–206.

(50) Bernardi, F.; Forlani, L.; Todesco, P. E.; Colonna, F. P.; Distefano, G. *J. Electron Spectrosc. Relat. Phenom.* **1976**, *9*, 217–226.

(51) Cooper, D. L.; Wright, S. C.; Gerratt, J.; Raimondi, M. *J. Chem. Soc., Perkin Trans. 2* **1989**, 263–267.

for the selenazole moiety. Although past thiazole studies do not in general deal with electron distribution, in those cases where results of population analyses are reported[36,49,51] they are in qualitative agreement with those of the present work. Results presented here are also consistent with those obtained from the more extensive computational literature on thiophene. Henriksson-Enflo[52] reviewed the results of 26 semiempirical and ab *initio calculations on thiophene. With one exception[53] these* calculations showed that a positive charge was present on the thiophene sulfur atom. As in both the thiazole and selenazole rings, the positive charge on the heteroatom was due to π-bonding with adjacent carbon atoms.

The significant positive charge calculated for the sulfur and selenium atoms supported an electrostatic origin for the heteroatom–oxygen interaction in the thiazole and selenazole nucleosides. We thus examined the electrostatic properties of the thiazole and selenazole heterocycles shown in Figure 3a in greater detail by computation of molecular electrostatic potentials (MEPs).[54] Point charges obtained from the Mulliken population analysis are subject to the well-known limitations of the method.[41] The Mulliken population analysis is based on the assumption that the overlap electron population is shared equally between the two participating centers. The resulting "point" charge associated with each atomic center makes no allowance for an anisotropic distribution of electron density.[41,47] MEPs representing the interaction between a positive test charge and the charge distribution computed directly from the molecular wave function avoid this problem.[54] MEPs obtained in this fashion provide a more accurate picture of the fragment's electrostatic environment as "seen" by approaching electrophiles and nucleophiles.

Figure 4 shows a MEP map calculated from the wave function of a 6-31G* geometry-optimized structure of the thiazole ring. The positive equipotential surface has a substantial bulge at the sulfur atom and is maximally displaced from the sulfur at positions roughly along the backsides of the sulfur–carbon bonds (top). The figure also shows lobes of negative electrostatic potential adjacent to the sulfur atom normal to the plane of the thiazole ring. This negative equipotential surface envelops the thiazole ring from both sides of the ring plane, making its closest approach in the vicinity of the nitrogen lone pair of electrons (bottom). Maps obtained from STO-3G and 3-21G* basis sets show very similar features.

The shapes of these equipotential surfaces are consistent with the findings of Rosenfeld et al.[4] The geometries of 69 crystal structures containing intermolecular nonbonded close contacts between a divalent sulfur and either a nucleophile or an electrophile were examined. The study showed that nucleophiles tend to approach the sulfur atom in the plane of the two sulfur bonds, approximately along the backside of these bonds. Electrophiles were observed to approach the sulfur atom roughly perpendicular to this plane. Similar results were observed for selenium contacts.[2] This pattern of approach would be predicted for the thiazole sulfur on the basis of the anisotropy of the MEP around this heteroatom. In particular, in the thiazole nucleosides, an intramolecular approach to the thiazole sulfur by the nucleophilic furanose oxygen would be expected. To test this hypothesis, computations were carried out on model fragments containing both the thiazole ring and a divalent oxygen. These results are presented next.

B. Core Fragments. Model thiazole and selenazole nucleoside fragments containing an analogue of the furanose O1' oxygen were derived from the crystal structures of tiazo- and selenazofurin (Figure 3b). These "core fragments" contain the minimum structural features common to all the thiazole and selenazole nucleosides. The initial value of the "glycosidic" torsion angle for each fragment was set equal to that of the corresponding crystal structure. The entire fragment was then subjected to full geometry
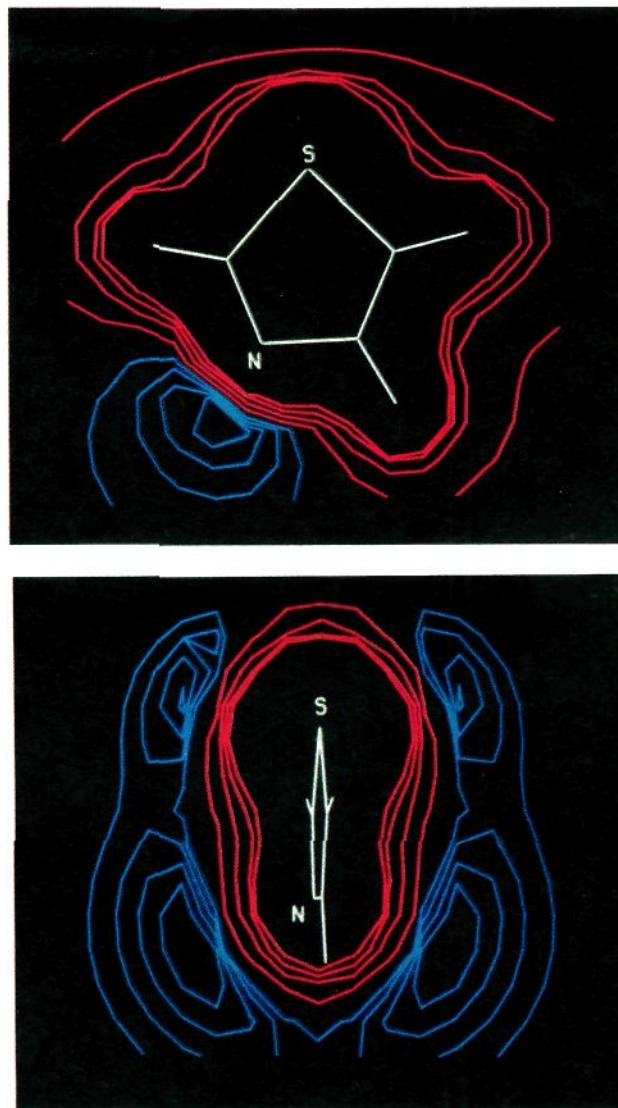
(52) Henriksson-Enflo, A. Theoretical Calculations on Thiophenes. In *Thiophene and its Derivatives*; Gronowitz, S., Ed.; Wiley: New York, 1985; pp 215–259.

(53) Defina, J. A.; Andrews, P. R. *Int. J. Quantum Chem.* **1980**, *XVIII*, 797–810.

(54) Politzer, P.; Truhlar, D. G. *Chemical Applications of Atomic and Molecular Electrostatic Potentials*; Plenum: New York, 1981; Chapter 1.
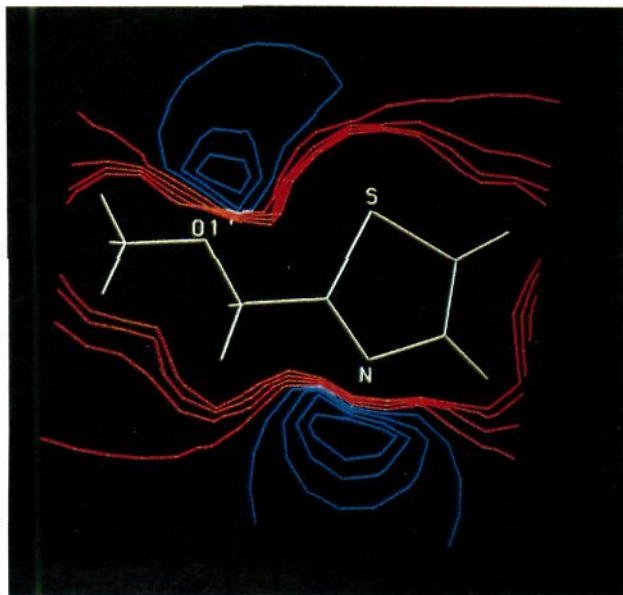

Figure 4. Molecular electrostatic isopotential maps for the isolated thiazole heterocycle. Positive values of the potential are contoured in red and negative values in blue. The map is contoured in the plane (top) and normal to the plane (bottom) of the ring. The heterocycle was subjected to a full geometry optimization using the 6-31G* basis set and the map computed from the resulting wave function (RHF/6-31G*//6-31G* level). The upper map is contoured from −0.02 to −0.08 au in steps of −0.02 au and from 0.02 to 0.14 au in steps of 0.04 au. The lower map is contoured from −0.08 to −0.014 au in steps of −0.002 au and from 0.008 to 0.098 au in steps of 0.03 au.

optimization at the STO-3G level. A 3-21G* wave function was also obtained for the thiazole fragment via a single-point calculation on the STO-3G optimized geometry. The geometries of the optimized thiazole and selenazole fragments are illustrated in Figure 3, c and d, along with the associated STO-3G Mulliken point charges for the heteroatoms.

In Figure 3, c and d show that, in both cases, the optimized geometry maintains the close heteroatom oxygen contact. The S–O and Se–O distances are 3.01 and 3.05 Å, respectively. Comparison of the net atomic charges on the thiazole and selenazole ring heteroatoms in the core fragments with those obtained from the isolated fragments (Table II) show little change. Specifically, the sulfur and selenium atoms maintain their positive charges while the nitrogen atom in each ring remains negative. Further, as expected, the extracyclic oxygen in both fragments carries a substantial negative charge. The net orbital overlap population between the thiazole sulfur and the extracyclic oxygen,

Figure 5. Molecular electrostatic isopotential map of the thiazole nucleoside core fragment shown in Figure 3b. Positive values of the potential are contoured in red and negative values in blue. The map is contoured in the plane of the thiazole ring, O1′ lying approximately 0.5 Å behind this plane. The map was computed from a 3-21G* single-point computation on the STO-3G minimized core fragment (Figure 3c, RHF/3-21G*//STO-3G level). Contours are from ±0.01 to ±0.07 au in steps of ±0.02 au.

obtained from the single point 3-21G* computation on the STO-3G minimized fragment, is 0.013. This value indicates little if any sulfur–oxygen covalent bonding. These observations together support an electrostatic interpretation of the heteroatom–oxygen interaction.

The electrostatic origin of the heteroatom–oxygen interaction is well illustrated by a MEP map of the thiazole fragment shown in Figure 3c. This map is computed from the 3-21G* wave function and is illustrated in Figure 5. The MEP about the thiazole end of the fragment is quite similar to that obtained for the isolated thiazole ring (Figure 4). The map further shows a lobe of negative potential in the vicinity of the O1′ oxygen lone pair. This lobe abuts the region of positive potential about the thiazole sulfur and is maximally displaced from the large region of negative potential about the thiazole nitrogen.

Thus, examination of both net charges and isopotential surfaces leads to the hypothesis that an attractive electrostatic interaction exists between the positively charged thiazole sulfur atom and the negatively charged O1′ oxygen. These results also indicate that there exists a simultaneous electrostatic repulsion between the N3 nitrogen and the O1′ oxygen atoms. Hence, the close sulfur–oxygen and selenium–oxygen contacts seen in tiazofurin and selenazofurin arise from both attractive and repulsive intramolecular electrostatic interactions. These interactions would be expected to produce barriers to rotation about the C–glycosidic bonds in the thiazole and selenazole nucleosides. In an effort to estimate both the magnitudes of such barriers and the factors which influence them, a series of progressively more realistic nucleoside fragments were examined. The energies of these fragments as a function of glycosidic torsion angle were computed using semiempirical methods. Results of these computations follow.

V. Semiempirical Calculations

Semiempirical calculations were performed on a number of model fragments. Simple fragments were examined first to test the consistency of the ab initio and semiempirical results. More complex fragments were then examined in order to quantify the barrier to rotation about the glycosidic bond and to ascertain what if any modulating effects would be produced by the rest of the
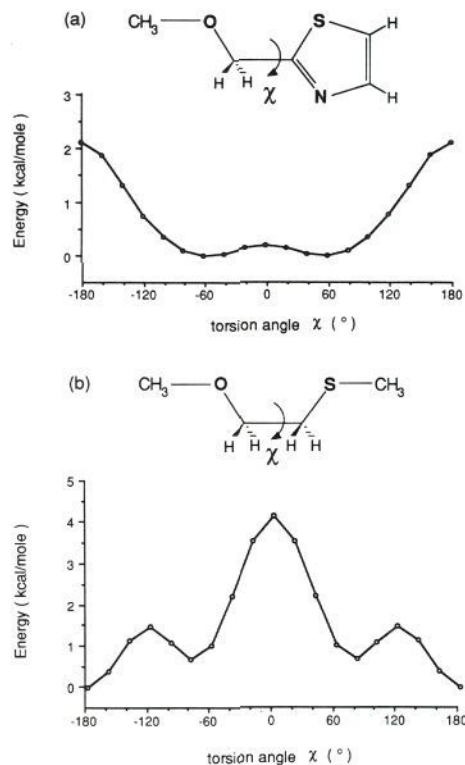

Figure 6. (a) Energy as a function of C–glycosidic torsion angle χ in the thiazole nucleoside core fragment. The figure above the plot illustrates the fragment used in the computation at $\chi = 0°$. The arrow indicates the rotation about χ required to generate the curve. The value of χ was incremented in 20° steps, fixed, and the remainder of the fragment subjected to full geometry optimization using the MNDO Hamiltonian. (b) Energy as a function of C–glycosidic torsion angle χ in the modified fragment lacking the conjugated ring. The values shown were computed as described for (a).

ribose ring on the electrostatic interaction.

A. Core Fragment. Figure 6a shows the results of an MNDO calculation performed on the "core fragment" defined above. The figure shows the calculated energy of the fully optimized fragment as a function of torsion angle χ (see Methods). The curve shows a broad minimum between $\chi = -60°$ and $\chi = 60°$ with a small ~0.2-kcal/mol hump at 0°, corresponding to the point where the sulfur and oxygen atoms are cis-planar to one another. This hump is unexpectedly low based solely on steric considerations, again supporting an attractive sulfur–oxygen interaction. At $\chi = 180°$, when the nitrogen and oxygen atoms are cis-planar, there is a 2.1-kcal/mol barrier.

As with the ab initio calculation, the results of this computation assign large positive and negative charges to the thiazole sulfur and nitrogen atoms, respectively ($Q_S = +0.381$, $Q_N = -0.199$). Population analysis shows that these charges result from π-bonding induced delocalization, as in the ab initio results. Also, the oxygen atom in the fragment corresponding to the O1′ oxygen in tiazofurin carries a significant negative charge ($Q_O = -0.357$). The fact that both the nitrogen and oxygen atoms are negatively charged suggests that the barrier at 180° is caused by electrostatic repulsion between these two atoms when they are cis-planar. The broad minimum centered at $\chi = 0°$, when the sulfur and oxygen atoms are cis-planar, results from an electrostatic attraction between these two atoms. This interpretation follows more rigorously from an analysis of the energy components of the Hamiltonian of the system. Energy partitioning[43,44] shows that, as the fragment is rotated from the 180° conformation (S–O trans) to the 0° conformation (S–O cis), the repulsive Coulombic components of the sulfur–oxygen interaction energy increase. These are the nuclear–nuclear and electron–electron interaction energies. The magnitude of the attractive Coulombic component of the sulfur–oxygen interaction also increases, but is opposite in sign to
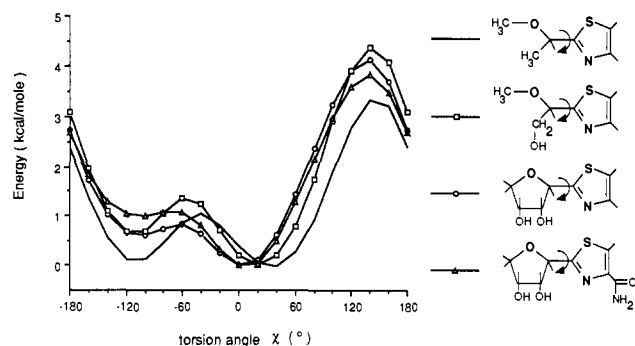
S-O and Se-O Interactions

J. Am. Chem. Soc., Vol. 114, No. 7, 1992 2319

Figure 7. Energy as a function of C–glycosidic torsion angle χ in extended thiazole nucleoside fragments of increasing size, illustrated at right. Arrows indicate rotation about χ in each fragment. The MNDO-based computations were performed as described for Figure 6a.

the repulsive components. This attractive component is the electron–nuclear interaction, the interaction between the sulfur electron density and the oxygen nucleus and vice versa. The total change in energy with respect to these three components is negative by $\sim$3 kcal/mol. This indicates that, at $\chi = 0°$, the attractive component of the sulfur–oxygen interaction outweighs the combination of the two repulsive components. Thus the $\chi = 0°$ conformer (S–O cis) is energetically preferred with respect to the sulfur–oxygen interactions. For the nitrogen–oxygen interactions the situation is reversed. At $\chi = 180°$ (N–O cis) the repulsive components exceed the attractive component, forcing the thiazole nitrogen trans to the oxygen. Thus, the semiempirical method indicates that the combination of attractive S–O and repulsive N–O electrostatic interactions are key factors leading to the broad energy minimum centered at 0° for this fragment.

Our ab initio calculations showed that the thiazole ring system allowed electron delocalization, resulting in the net positive charge on the sulfur atom. In order to assess the importance of the thiazole ring on the sulfur–oxygen interaction in tiazofurin, we performed an MNDO calculation on a modification of the core fragment in which the sulfur atom was no longer a part of a conjugated system. The results of this computation are shown in Figure 6b. The curve describing the energy of this fragment as a function of torsion angle was computed in the same manner as that shown in Figure 6a. Population analysis shows very little π-bonding between the sulfur and the adjacent carbon atoms in this environment. This results in a much smaller positive charge than that seen on the sulfur atom in the thiazole ring ($Q_S = 0.072$, $Q_O = -0.355$). The attractive electron–nuclear component of the sulfur–oxygen interaction is decreased and the repulsive terms now dominate the Hamiltonian at $\chi = 0°$. Because of the loss of the attractive electrostatic interaction, there is now a sizable steric barrier to rotation centered at $\chi = 0°$, when the sulfur and oxygen atoms are cis-planar. Further, the absence of the negatively charged nitrogen in this fragment removes the previously observed barrier at $\chi = 180°$.

These computations confirm that generation of a substantial positive charge on the sulfur atom is made possible by a strong electron-withdrawing environment, in this case provided by the thiazole ring. Delocalization in the ring creates a positive charge on the sulfur sufficient to produce an attractive electrostatic interaction with the extracyclic oxygen. Further, the ring provides a repulsive interaction between the negatively charged thiazole nitrogen and this oxygen. These interactions account for, respectively, the broad energy minimum centered at 0° and the barrier at 180° seen in the core fragment.

B. Extended Fragments. In order to determine the influence of additional components of the tiazofurin molecule on the energy profile of the core fragment, MNDO calculations were carried out on extended fragments of increasing size (Figure 7). The conformation of the ribose portion of the fragments shown in Figure 7 was C3′ endo. Results for C2′ endo conformers are similar. Comparison of the plots in Figure 7 with that obtained from the core fragment (Figure 6a) shows several differences. The largest barrier to rotation is shifted from $\chi = 180°$ to $\chi = 140°$.
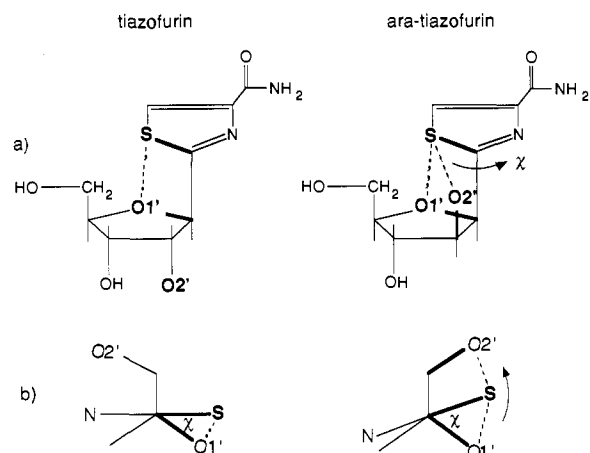

Figure 8. (a) Tiazofurin and *ara*-tiazofurin. Dotted lines indicate the close contacts observed in the crystal structures. The arrow indicates the larger value of the C–glycosidic torsion angle χ observed in *ara*-tiazofurin. (b) Projections down the C–glycosidic bonds of the structures shown in part a, with part of the sugar rings removed. The C–glycosidic torsion angle is labeled in each projection. Bonds to atoms involved in close contacts are drawn as heavy lines and correspond to the heavy-lined bonds indicated in part a.

The size of this barrier is increased to $\sim$4 kcal/mol for the fragments containing the 2′ hydroxyl oxygen. A smaller barrier also occurs at $\chi = -60°$. Energy partitioning indicates that the additional height of the 140° barrier is primarily due to a decrease in exchange and resonance interactions across the C–glycosidic bond in this configuration. The shift in the barrier location is a result of the modulating influence of a sulfur-H2′ interaction. However, the major component of this barrier remains the net repulsive N3–O1′ electrostatic interaction. In contrast, energy minima for the extended fragments are observed at torsion angles between 0° to $\sim$35°. This range encompasses the values of χ observed for most of the thiazole nucleosides (Table I). Energy partitioning again reveals that these conformations are stabilized by the attractive electrostatic interaction between S and O1′. The similarity between the curves shown in Figure 7 suggests that the C2′ carbon and its substituents have the greatest modifying effect on the energies of the extended fragments. However, the C2′ carbon and its substituents only modulate the sulfur–oxygen and nitrogen–oxygen interactions. The ultimate conformational effect of these interactions remains the same: to bring the thiazole sulfur cis to the ribose oxygen.

VI. *ara*-Tiazofurin

As mentioned earlier, the crystal structure of *ara*-tiazofurin exhibits only a moderately close S–O1′ contact compared to that observed in the other thiazole nucleosides. This conformational "exception" can be explained in terms of two competing nonbonded sulfur–oxygen interactions.[15]

Figure 8a compares tiazofurin and *ara*-tiazofurin, emphasizing the different placements of the O2′ hydroxyl oxygens. The crystal structure of *ara*-tiazofurin shows marginally close S–O1′ and S–O2′ interactions (dotted lines), with a correspondingly larger C–glycosidic torsion angle χ (arrow). This is further illustrated in Figure 8b, in which the two structures are viewed in projection down the C–glycosidic bond, with only a part of the sugar ring shown. Electrostatic equipotential surfaces corresponding to these views (Figure 9) indicate the reason for the difference in χ between the two molecules.

Figure 9 shows views down the glycosidic bonds in the crystal structures of tiazofurin and *ara*-tiazofurin. Again, only part of the sugar ring is shown for each structure. Maps were obtained from single point calculations using the 3-21G* basis set and the crystal structure geometries of the two molecules.[14,15] The tiazofurin structure (top) exhibits the familiar close S–O1′ contact with a corresponding glycosidic torsion angle of 30.7°. In *ara*-tiazofurin (bottom), the O2′ hydroxyl group is located on the opposite side of the furanose ring, placing it as well as O1′ close
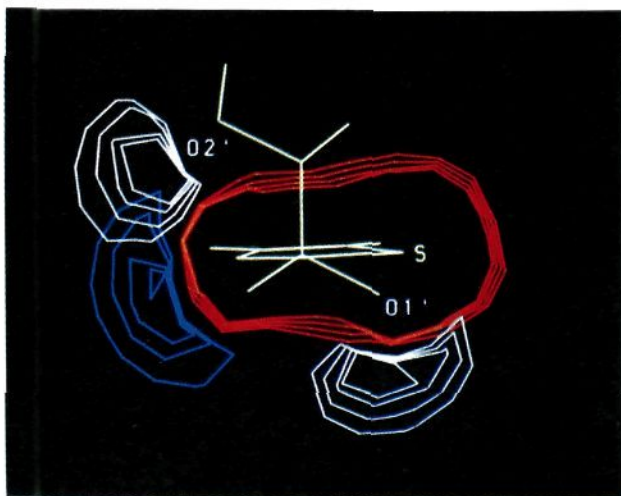
Figure 10. Energy as a function of C–glycosidic torsion angle χ in an *ara*-tiazofurin model fragment (top) and a tiazofurin model fragment (bottom). The MNDO-based computations were performed as described for Figure 6a. The arrow indicates the shift in related minima between the two structures, with a corresponding increase in the value of χ predicted for *ara*-tiazofurin.

compete, the former "pulling" the thiazole ring into the higher glycosidic torsion angle (Figure 8b).

VII. Summary

Computational studies indicate that close sulfur–oxygen and selenium–oxygen contacts observed in the thiazole and selenazole nucleosides are the result of nonbonded interactions. Ab initio studies show that sulfur and selenium heteroatoms in thiazole and selenazole rings have a net positive charge. This positive charge results from donation of Pz electrons to the π system of the heterocycle, and is distributed anisotropically in a manner consistent with observed sulfur and selenium intermolecular contacts. The S/Se–O interaction is interpreted as an electrostatic attraction between a negatively charged furanose oxygen and a positively charged sulfur or selenium. MNDO computations on thiazole nucleoside-like fragments exhibit an approximately 4-kcal/mol barrier to rotation about the C–glycosidic bond. This barrier results from the attractive S–O1′ interaction as well as a repulsive N–O1′ interaction. Both of these nonbonded interactions constrain rotation about the C–glycosidic bond, favoring the conformation in which the thiazole sulfur and furanose oxygen are cis. Similar constraints are expected in the selenazole nucleosides as well. Kinetic and modeling studies indicate that such constraints may influence the binding of both tiazo- and selenazofurin, in the form of the active dinucleotides TAD and SAD, to both the target enzyme (IMPd) and to other dehydrogenases.[26] The specificity of TAD and SAD for these enzymes may be either enhanced or diminished, depending upon the degree to which the heteroatom–oxygen interaction is maintained by the particular binding site.[26] In either case, the nonbonded interactions studied here clearly have important biological implications. It is likely that S/Se–O interactions play an equally important role in other classes of compounds as well. The effects of these noncovalent interactions on the conformations and, thus, on the chemistries of other systems deserve further study.

Figure 9. Molecular electrostatic isopotential maps for tiazofurin (top) and *ara*-tiazofurin (bottom). Views are down the C–glycosidic bond in each structure and correspond to those illustrated in Figure 8b. Part of the sugar ring is removed in each structure for clarity. Positive values of the potential are contoured in red and negative values in blue and white. Each map is contoured in two parallel planes normal to the C–glycosidic bond and separated by 3 Å. The front plane (red and blue contours) intersects the thiazole N3 and S. The back plane (white contours) approximately intersects O1′ and O2′. For clarity, positive values of the potential are not contoured in the back plane. Each map was obtained from a 3-21G* single-point computation using the crystal-structure geometry of the corresponding molecule (RHF/3-21G*// *experimental level*). Each map is contoured from −0.04 to −0.7 au in steps of −0.01 au and from 0.04 au to 1.0 au in steps of 0.02 au.

to the thiazole sulfur. The thiazole ring is rotated such that χ has a value of 55.2°, placing the thiazole sulfur roughly midway between the O1′ and O2′ oxygen atoms.[15] It appears that the sulfur atom in the ara compound is involved in an attractive interaction with the O2′ oxygen as well as with the O1′ oxygen. We tested this hypothesis by performing MNDO calculations on an ara-like fragment. The results of this calculation are shown in Figure 10. The minimum energy torsion angle shifts from ~20° for the tiazofurin-like fragment to ~50° for *ara*-tiazofurin. This is in good agreement with the 55.2° torsion angle seen in the *ara*-tiazofurin crystal structure.[15] Analysis of energy partitioning in this calculation shows that there is, in fact, an additional attractive electrostatic interaction between the thiazole sulfur and the extracyclic O2′ oxygen. The S–O2′ and S–O1′ interactions
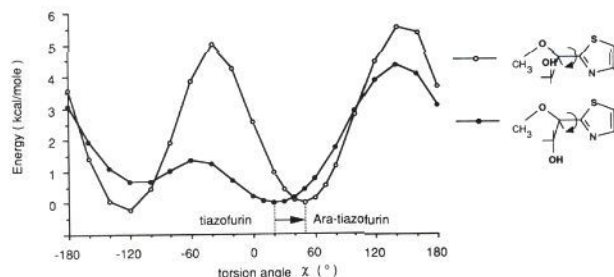
(55) *Browse Quantum Chemistry Database System User's Guide.* Frisch, M. J., Ed.; Gaussian, Inc.: Pittsburgh, PA, 1988.